Electrochemistry

A Mesoporous/Crystalline Composite Material Containing Tin Phosphate for Use as the Anode in Lithium-Ion Batteries**

Eunjin Kim, Dongyeon Son, Tae-Gon Kim, Jaephil Cho,* Byungwoo Park,* Kwang-Sun Ryu, and Soon-Ho Chang

Since Idota et al. first discovered in 1997 that Sn anodes containing amorphous $SnB_{0.56}P_{0.4}Al_{0.42}O_{3.46}$ have a capacity of about 600 mAh g^{-1}, compared to a value of 372 mAh g^{-1} for

[*] E. Kim, Prof. Dr. J. Cho
Department of Applied Chemistry
Kumoh National Institute of Technology
Gumi 730-701 (South Korea)
Fax: (+82) 54-467-4477
E-mail: jpcho@kumoh.ac.kr

D. Son, T.-G. Kim, Prof. Dr. B. Park
School of Materials Science and Engineering
and Research Center for Energy Conversion and Storage
Seoul National University, Seoul 151-744 (South Korea)
Fax: (+82) 2-883-8197
E-mail: byungwoo@snu.ac.kr

Dr. K.-S. Ryu, Dr. S.-H. Chang
Power Source Device Team, Electronics & Telecommunications
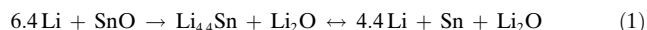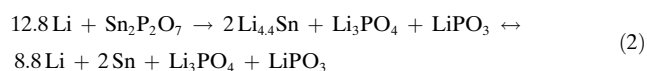Research Institute (ETRI), Daejeon 305-350 (Korea)

graphite,[1] many studies on Sn-based materials for use as anode materials have been performed.[2–4] Courtney et al. have reported the overall reaction of Sn-containing anode materials using SnO as Equation (1).[2]

$$6.4\,Li + SnO \rightarrow Li_{4.4}Sn + Li_2O \leftrightarrow 4.4\,Li + Sn + Li_2O \qquad (1)$$

The tin atoms aggregate during cycling, and the Li–Sn alloys embedded in the Li_2O matrix exhibit rapid loss of capacity.

The presence of substantial amounts of other "spectator atoms", such as the B and P atoms in Sn_2BPO_6, apparently prevents Sn aggregation.[2] However, these materials show an initial capacity of about 500 mAh g^{-1}, with a relatively high irreversible capacity of about 500 mAh g^{-1} during the first cycle. Xiao et al. prepared a crystalline $Sn_2P_2O_7$ phase, and proposed the decomposition reaction [Eq. (2)].[3]

$$12.8\,Li + Sn_2P_2O_7 \rightarrow 2\,Li_{4.4}Sn + Li_3PO_4 + LiPO_3 \leftrightarrow$$
$$8.8\,Li + 2\,Sn + Li_3PO_4 + LiPO_3 \qquad (2)$$

However, the irreversible capacity of this material is high (523 mAh g^{-1}), and the initial capacity of 544 mAh g^{-1} decreases quickly even at a low current (C) rate (20 mA g^{-1}). Behm and Irvine have reported that crystalline $Sn_2P_2O_7$ (obtained by heating $SnHPO_4$ to 550 °C) exhibits an initial charge capacity of 519 mAh g^{-1}, which decreases rapidly to 148 mAh g^{-1} after 30 cycles.[4] They proposed that lithium phosphates (Li_3PO_4 and $LiPO_3$), as reaction products, could not play a similar role as Li_2O in the SnO system, which is as a "glue" that keeps the Li–Sn particles mechanically connected during the large volume changes during alloying/dealloying. The mesoporous SiO_2/SnO_2 composite reported by Chen et al.[5] has a good cycling stability, as evident from the cyclic voltammogram recorded with a single-powder microelectrode.

Herein we report the synthesis of a mesoporous tin phosphate/crystalline $Sn_2P_2O_7$ composite as a novel anode material. This material has the highest initial charge capacity (721 mA h g^{-1}) of the known tin-based anode materials, and shows an excellent cycling stability. The mesoporous structure was incorporated to improve the structural/electrochemical properties by alleviating the volume change of the tin during the alloying/dealloying process.

Figure 1 shows small-angle X-ray scattering (SAXS) patterns of the mesoporous tin phosphates prepared in the presence of cetyltrimethylammonium bromide (CTAB, $CH_3(CH_2)_{15}N(CH_3)_3Br$) as a structure-directing agent, before and after annealing at 400 °C for 8 h. The three resolved peaks indexed as (100), (110), and (200) confirm a well-ordered hexagonal mesoporous structure.[6,7] The intense (100) peak at $2\theta = 2.18° \pm 0.09°$ of the as-synthesized mesoporous tin phosphate corresponds to a d spacing of 4.0 ± 0.2 nm (from $2d \sin\theta = \lambda$), with a nearest-neighbor distance of 4.7 ± 0.2 nm. The high-angle XRD pattern shown in the inset of Figure 1a indicates the formation of crystalline $SnHPO_4$ with a space group $P2_1/c$ (monoclinic).[8]

The appearance of small-angle diffraction peaks corresponding to a hexagonal structure for the annealed meso-
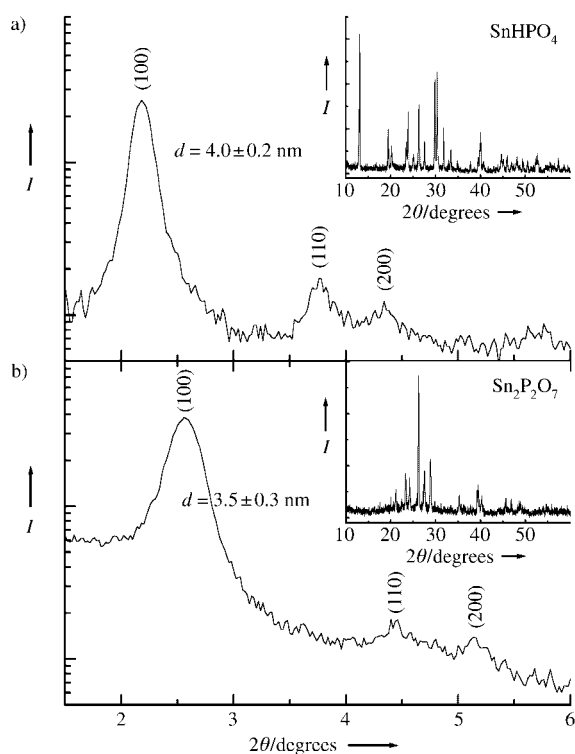
Figure 1. Small-angle X-ray scattering patterns of: a) as-prepared mesoporous tin phosphate/SnHPO₄ composite, and b) mesoporous tin phosphate/Sn₂P₂O₇ composite after annealing at 400°C for 8 h. The high-angle X-ray diffraction patterns of (a) and (b) are shown in the insets (*I*: intensity).

Figure 2. TEM images of: a) as-synthesized mesoporous tin phosphate, and b) mesoporous tin phosphate after annealing at 400°C for 8 h.

Figure 3. Representative nitrogen adsorption and desorption isotherms for the mesoporous tin phosphate/Sn₂P₂O₇ composite. The corresponding BJH distribution is shown in the inset (*v*: adsorbed volume; *D*: pore diameter; P/P_0: relative pressure).

porous sample indicates that the mesostructure is preserved upon removal of the CTAB surfactant after annealing. However, the meso periodicity is contracted; the corresponding d spacing of the annealed mesoporous tin phosphate is 3.5 ± 0.3 nm.[6,9,10] The high-angle XRD pattern of the annealed sample clearly shows the presence of $Sn_2P_2O_7$ (inset of Figure 1b).[4] The crystal size of the sample both before and after annealing, calculated using the Scherrer formula, was estimated to be approximately 100 nm,[11] which is two orders of magnitude larger than the wall thickness of the pure mesoporous phase (ca. 1 nm). These results indicate the formation of a mesoporous tin phosphate mixed with a crystalline phase.

Figure 2 shows the TEM micrographs of the samples before and after annealing, and clearly shows the presence of hexagonal mesoporous materials. The corresponding d spacings (by TEM) are approximately 3.8 nm before annealing and about 3.3 nm after annealing; these values are consistent with the SAXS data. The TEM image of the annealed tin phosphate clearly shows that the hexagonal mesostructure is preserved after heating to 400°C.[12,13] The light stripes in Figure 2 can be considered as projections of the mesopore channels, whereas the dark lines are from the tin phosphate walls.[14]

The nitrogen-adsorption isotherm of the annealed sample, which has a Brunauer–Emmett–Teller (BET) surface area of 75.6 m²g⁻¹, is shown in Figure 3. The measured surface area is smaller than that of other mesoporous metal oxides reported
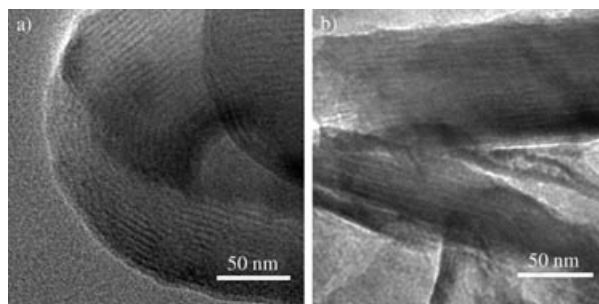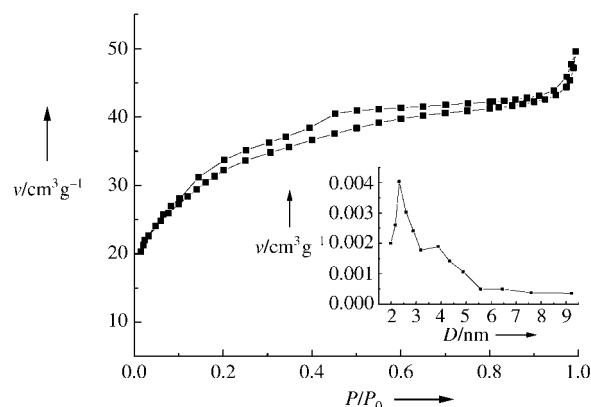
in the literature because of the coexistence of a crystalline phase. The nitrogen isotherm curve of the mesoporous tin phosphate/$Sn_2P_2O_7$ composite has a well-defined step, which is characteristic of framework-confined mesopores.[15–17] A rough estimation of the mass ratio for mesoporous tin phosphate versus crystalline $Sn_2P_2O_7$ is approximately 1:3. (This ratio was estimated from the BET surface areas of both the mesoporous tin phosphate and crystalline $Sn_2P_2O_7$ by considering the pore diameter and wall thickness.) As shown in the inset of Figure 3, the average pore size in the annealed sample is approximately 2.3 nm (Barrett–Joyner–Halenda (BJH) analysis), which is consistent with the SAXS and TEM data (Figures 1 and 2, respectively).

Figure 4 compares the voltage profiles of pure crystalline $Sn_2P_2O_7$ and mesoporous tin phosphate/$Sn_2P_2O_7$ composite anodes, which were cycled up to the 30th cycle at a rate of 144 mAg⁻¹ (first cycle at 72 mAg⁻¹) between 2.5 and 0 V. The crystalline $Sn_2P_2O_7$ anode shows a large initial irreversible capacity (389 mAhg⁻¹) and poor retention property after 30 cycles (from 704 to 146 mAhg⁻¹). On the other hand, the mesoporous tin phosphate/$Sn_2P_2O_7$ composite anode shows an initial charge capacity of 721 mAhg⁻¹, which is much larger than the tin phosphate anodes reported previously.[1–4] Moreover, the irreversible capacity of the sample during the first cycle is 297 mAhg⁻¹, which is far superior to the previous
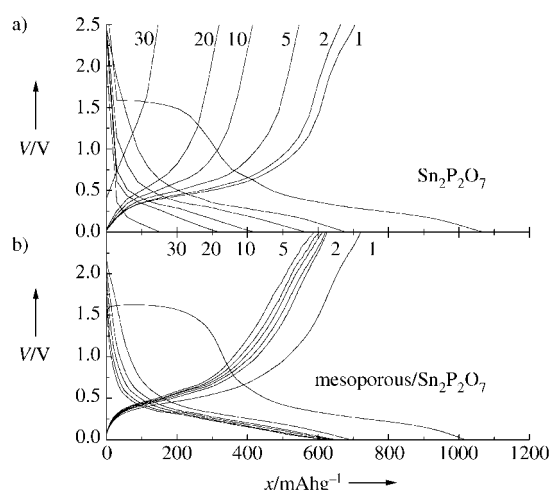
Figure 4. Voltage profiles of a) a crystalline $Sn_2P_2O_7$ anode and b) a mesoporous tin phosphate/$Sn_2P_2O_7$ composite anode in coin-type half-cells during the 1st, 2nd, 5th, 10th, 20th, and 30th cycles between 2.5 and 0 V. The C rate was maintained at 144 mAg^{-1} (first cycle at 72 mAg^{-1}; V: cell potential).
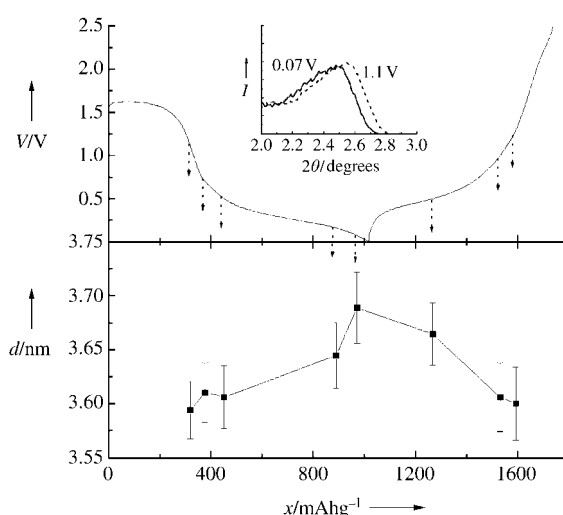

Figure 5. Plots of: a) cell potential of the mesoporous tin phosphate/$Sn_2P_2O_7$ composite anode in coin-type half-cells during the first discharging and charging, and b) the corresponding d spacing of the composite electrode at the cell potential indicated by the arrow. The inset shows small-angle X-ray diffraction patterns of the electrode at 1.1 V and 0.07 V (V: cell potential; d: d spacing; I: intensity).

studies on Sn-based oxides or alloys.[1–4] In addition, the mesoporous tin phosphate/$Sn_2P_2O_7$ composite exhibits excellent cyclability: the retentive capacity up to 30 cycles is 587 mAh g^{-1}. This result indicates that the mesoporous tin phosphate plays a significant role in retaining the capacity. The XRD patterns of the cycled electrodes show that the crystalline $Sn_2P_2O_7$ peaks disappear during the first discharge (at ca. 1.1 V) and give only weak and broad diffraction patterns. The amorphous or nanocrystalline electrode in the phosphate matrix may prevent formation of large Sn clusters.[18,19] The measured discharge and charge capacities are higher than the theoretical values (834 mAh g^{-1} and 572 mAh g^{-1}, respectively).[3] The formation of a solid-electrolyte interface layer[20] and a reversible lithium phosphate matrix[18] may induce these higher values, although the exact mechanisms need to be identified.

Figure 5 shows the cell potential of the mesoporous tin phosphate/$Sn_2P_2O_7$ composite anodes during the first discharging/charging together with the corresponding changes of the mesopore periodicity. Surprisingly, the d spacing expands and shrinks with Li alloying/dealloying. We believe that the lithium-tin phosphates form a flexible, three-dimensional mesoporous framework such that the mesopores do not collapse during discharge and charge. The cutoff voltage in Sn-based oxides has been typically limited to 1.2 V as a consequence of rapid tin aggregation above 1.2 V. The mesopores play an important role in reducing possible aggregation of Sn particles, and act as a "buffer zone" which accommodates the volume change of the Sn phase during Li alloying/dealloying. More detailed experiments with the optimum microstructures are currently underway to improve the electrochemical properties shown in Figure 4.

In conclusion, our mesoporous tin phosphate/$Sn_2P_2O_7$ composite anode shows superior electrochemical properties, such as a large initial capacity (ca. 721 mAh g^{-1}) and excellent cyclability (ca. 587 mAh g^{-1} at the 30th cycle). Our approach

for enhancing the structural stability of tin phosphate is to incorporate mesoporous structures as a buffer layer to alleviate the volume expansion of the tin phosphate anode during lithiation/delithiation. We believe that this novel mesoporous tin phosphate/$Sn_2P_2O_7$ composite has an enormous potential for use in Li-battery anode materials.

Experimental Section

The mesoporous tin phosphate/$SnHPO_4$ composite was prepared by mixing SnF_2 (6.0 g) and H_3PO_4 (13.8 g) and dissolving this mixture in distilled-deionized water (DDW, 40 mL). CTAB (5.5 g) was then dissolved in DDW (20 mL), and this solution was added to the first solution. The mixture was stirred at 40 °C for 1 h and then loaded into an autoclave and heated to 90 °C for 12 h. After cooling the mixture to room temperature, the precipitate was recovered by filtration, washed with distilled water and ethanol, and vacuum-dried at 100 °C for 10 h. The as-prepared powders (mesoporous tin phosphate/$SnHPO_4$ composite) were then annealed at 400 °C for 8 h to give the mesoporous tin phosphate/$Sn_2P_2O_7$ composite.

The procedure for assembling a coin-type half-cell with Li as an anode has been described in detail elsewhere.[21–24] The electrode consisted of 60 wt-% active materials, 20 wt-% Super P carbon black, and 20 wt-% poly(vinylidene fluoride). A mixture of ethylene carbonate/diethylene carbonate and 1M $LiPF_6$ salt was used as the electrolyte. The SAXS patterns were measured using Cu $K\alpha$ radiation (40 kV, 35 mA) on a Bruker Nanostar instrument. The nitrogen-adsorption isotherm was measured at 77 K with a Micromeritics ASAP 2010 analyzer.

[1] Y. Idota, T. Kubota, A. Matsufuji, Y. Maekawa, T. Miyasaka, *Science* **1997**, *276*, 1395.

[2] I. A. Courtney, W. R. Mckinnon, J. R. Dahn, *J. Electrochem. Soc.* **1999**, *146*, 59.

[3] Y. W. Xiao, J. Y. Lee, A. S. Yu, Z. L. Liu, *J. Electrochem. Soc.* **1999**, *146*, 3623.

[4] M. Behm, J. T. S. Irvine, *Electrochim. Acta* **2002**, *47*, 1727.

[5] F. Chen, Z. Shi, M. Liu, *Chem. Commun.* **2000**, 2095.

[6] G. Li, S. Bhosale, T. Wang, Y. Zhang, H. Zhu, J.-H. Fuhrhop, *Angew. Chem.* **2003**, *115*, 3948; *Angew. Chem. Int. Ed.* **2003**, *42*, 3818.

[7] T. Katou, B. Lee, D. Lu, J. N. Kondo, M. Hara, K. Domen, *Angew. Chem.* **2003**, *115*, 2484; *Angew. Chem. Int. Ed.* **2003**, *42*, 2382.

[8] M. L. E. Moubtassim, J. I. Corredor, J. M. Lloris, C. P. Vicente, J. L. Tirado, *J. Electrochem. Soc.* **2002**, *149*, A1030.

[9] C. Serre, A. Auroux, A. Gervassini, M. Hervieu, G. Ferey, *Angew. Chem.* **2002**, *114*, 1664; *Angew. Chem. Int. Ed.* **2002**, *41*, 1594.

[10] N. K. Mal, S. Ichikawa, M. Fujiwara, *Chem. Commun.* **2002**, 112.

[11] Y. Kim, J. Oh, T.-G. Kim, B. Park, *Appl. Phys. Lett.* **2001**, 78, 2363.

[12] M. Tiemann, M. Fröba, *Chem. Mater.* **2001**, *13*, 321, and references therein.

[13] K. G. Severin, T. M. Abdel-Fattah, T. J. Pinnavia, *Chem. Commun.* **1998**, 1471.

[14] M. Kruk, M. Jaroniec, T.-W. Kim, R. Ryong, *Chem. Mater.* **2003**, *15*, 2815.

[15] F. Schüth, W. Schmidt, *Adv. Mater.* **2002**, *14*, 629.

[16] S.-H. Baeck, K.-S. Choi, T. F. Jaramillo, G. D. Stucky, E. W. McFarland, *Adv. Mater.* **2001**, *13*, 11.

[17] F. Chen, Z. Shi, M. Liu, *Chem. Commun.* **2000**, 2095.

[18] P. Poizot, S. Laruelle, S. Grugeon, L. Dupont, J.-M. Tarascon, *Nature* **2000**, *407*, 496.

[19] N. Zheng, X. Bu, P. Feng, *Nature* **2003**, *426*, 428.

[20] D. Aurbach, A. Nimberger, B. Markovsky, E. Levi, E. Sominski, A. Gedanken, *Chem. Mater.* **2002**, *14*, 4155.

[21] J. Cho, Y. J. Kim, B. Park, *Chem. Mater.* **2000**, *12*, 3788.

[22] Y. J. Kim, H. Kim, B. Kim, D. Ahn, J.-G. Lee, T.-J. Kim, D. Son, J. Cho, Y.-W. Kim, B. Park, *Chem. Mater.* **2003**, *15*, 1505.

[23] J. Cho, Y. J. Kim, T.-J. Kim, B. Park, *Angew. Chem.* **2001**, *113*, 3471; *Angew. Chem. Int. Ed.* **2001**, *40*, 3367.

[24] J. Cho, Y.-W. Kim, B. Kim, J.-G. Lee, B. Park, *Angew. Chem.* **2003**, *115*, 1656; *Angew. Chem. Int. Ed.* **2003**, *42*, 1618.